


RESEARCH LETTER

Open Access



The western extension of the Balantak Fault revealed by the 2021 earthquake cascade in the central arm of Sulawesi, Indonesia

Andrean V. H. Simanjuntak¹, Kadek H. Palgunadi^{2,3}, Pepen Supendi^{1,4}, Umar Muksin⁵, Endra Gunawan⁶, Sri Widiyantoro^{6,7*} , Nicholas Rawlinson⁴, Mudrik R. Daryono⁸, D. Daryono¹, Dwikorita Karnawati¹, Nuraini R. Hanifa⁸, Cecep Pratama⁹ and Rachmah Ida¹⁰

Abstract

Two shallow earthquakes of moment magnitude 6.2 and 5.8 occurred in the central arm of Sulawesi on 26 July 2021 and 26 August 2021, respectively. The fault responsible for the earthquake had previously only been partially mapped, thus making further analysis of its characteristics crucial for the assessment of seismic hazard. In this study, we exploit data from a regional seismic network, relocate the associated seismicity using the double difference method with an updated velocity model, determine focal mechanisms from full-waveform inversion, and analyze the static stress changes caused by the mainshock. Our relocated hypocenters and focal mechanism solutions reveal two earthquake clusters, one at the Central Balantak Fault that exhibits normal slip on a SE–NW trending rupture, and the other at the West Balantak Fault, which exhibits dextral strike-slip motion on a SE–NW trending rupture. The additional static stress increase transferred by the Mw 6.2 mainshock may have triggered the subsequent Mw 5.8 event. A detailed assessment of previously unmapped faults in Central Sulawesi is essential for a more comprehensive understanding of seismic hazard in the region.

Keywords Earthquake, Fault, Focal mechanism, Static stress change

*Correspondence:

Sri Widiyantoro
ilikwidi@gmail.com

¹ Agency for Meteorology, Climatology, and Geophysics, Jakarta 10720, Indonesia

² Physical Science and Engineering, King Abdullah University of Science and Technology, Thuwal, Saudi Arabia

³ Geophysical Engineering Department, Institut Teknologi Sepuluh Nopember, Kampus ITS, Sukolilo, Surabaya 60111, Indonesia

⁴ Department of Earth Sciences – Bullard Labs, University of Cambridge, Cambridge CB30EZ, UK

⁵ Tsunami Disaster and Mitigation Research Center, Universitas Syiah Kuala, Banda Aceh, Aceh 23011, Indonesia

⁶ Global Geophysics Research Group, Faculty of Mining and Petroleum Engineering, Institut Teknologi Bandung, Bandung 40132, Indonesia

⁷ Faculty of Engineering, Maranatha Christian University, Bandung 40164, Indonesia

⁸ National Research and Innovation Agency, Jakarta 10340, Indonesia

⁹ Department of Geodetic Engineering, Universitas Gadjah Mada, Yogyakarta 55281, Indonesia

¹⁰ Department of Communication, Faculty of Social and Political Science, Universitas Airlangga, Surabaya 60286, Indonesia



© The Author(s) 2024. **Open Access** This article is licensed under a Creative Commons Attribution 4.0 International License, which permits use, sharing, adaptation, distribution and reproduction in any medium or format, as long as you give appropriate credit to the original author(s) and the source, provide a link to the Creative Commons licence, and indicate if changes were made. The images or other third party material in this article are included in the article's Creative Commons licence, unless indicated otherwise in a credit line to the material. If material is not included in the article's Creative Commons licence and your intended use is not permitted by statutory regulation or exceeds the permitted use, you will need to obtain permission directly from the copyright holder. To view a copy of this licence, visit <http://creativecommons.org/licenses/by/4.0/>.

Introduction

On 26 July 2021, a large Mw 6.2 earthquake occurred in the central arm of Sulawesi that generated significant ground shaking (between IV–VI on the Modified Mercalli Intensity (MMI) scale—see www.shakemap.bmkg.go.id) and caused severe damage to more than 25 houses. This earthquake was preceded by an Mw 5.7 foreshock that occurred eight hours before the mainshock. The Indonesian Agency for Meteorology, Climatology, and Geophysics (Badan Meteorologi, Klimatologi, dan Geofisika/BMKG) reported hundreds of aftershocks followed by the Mw 6.2 mainshock. One month later (26 August 2021), an Mw 5.8 earthquake occurred some

50 km to the west of the Mw 6.2 mainshock (Fig. 1). Focal mechanism solutions taken from the U.S. Geological Survey (USGS) reveal that the Mw 6.2 (26 July 2021) event occurred on a normal fault, while the Mw 5.8 (26 August 2021) event occurred on a strike-slip fault (Fig. 1). The different mechanisms of these two earthquakes raise questions about whether both events occurred on the same fault, and whether the later Mw 5.8 event was triggered by the Mw 6.2 mainshock.

Over the past decade, there have been two major destructive earthquakes in Central Sulawesi, the Mw 6.8 (29 May 2017) Poso earthquake (Daniarsyad et al. 2021) and the Mw 7.5 (28 September 2018) Palu earthquake

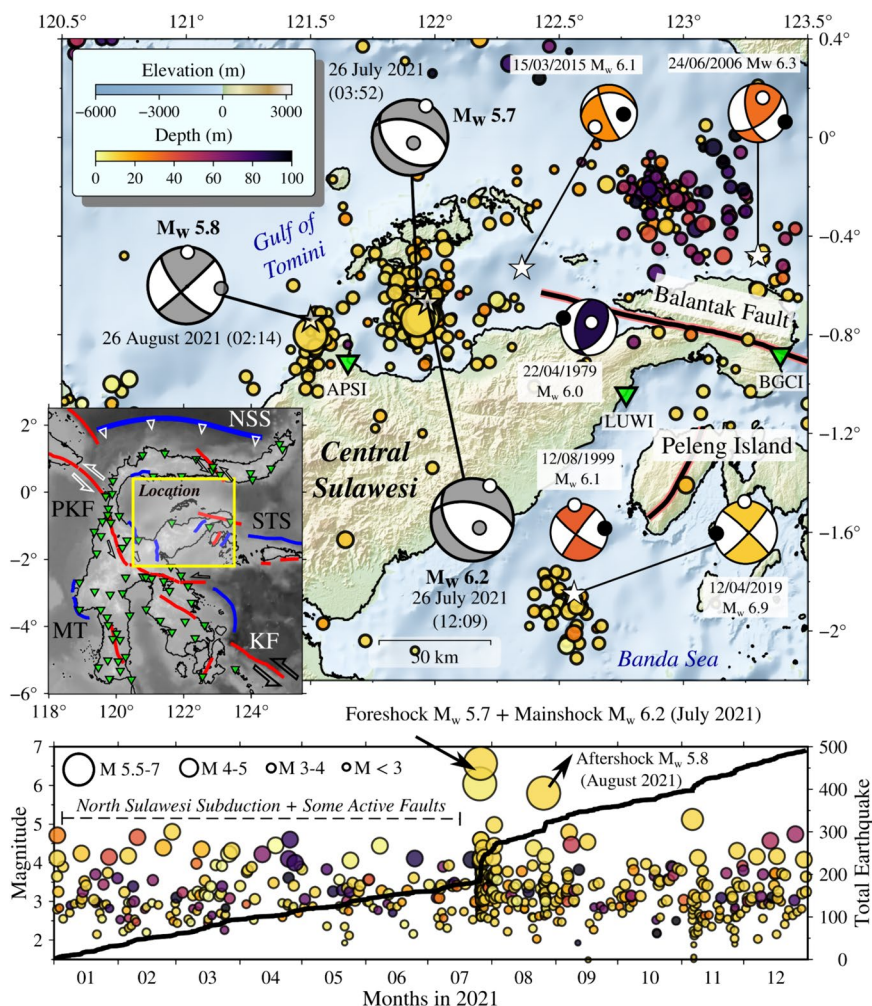


Fig. 1 The inset on the upper panel shows a tectonic map of Central Sulawesi that includes active faults (red lines) and known thrust faults (blue lines), with the North Sulawesi Subduction (NSS) zone, Palu-Koro Fault (PKF), Sula Thrust System (STS), Kendari Fault (KF), and Majene Thrust (MT) as the major fault systems. The study area is in Central Sulawesi (yellow square). The upper panel depicts the earthquake distribution in Central Sulawesi between January and December 2021. Two earthquakes (Mw 5.7 foreshock and Mw 6.2 mainshock) occurred on 26 July 2021 that have normal faulting mechanisms, and an Mw 5.8 earthquake with a strike-slip mechanism occurred one month later on 26 August 2021. The lower panel indicates the temporal evolution of the earthquake sequence overlaid with the cumulative number of earthquakes, magnitudes and the foreshock, mainshock, and associated aftershocks

([Bao et al. 2019](#); [Natawidjaja et al. 2020](#); [Supendi et al. 2020](#)). Other recent earthquakes based on GCMT with $M_w \geq 6$ include the May 28, 1977, M_w 6.1; April 22, 1979, M_w 6.0; August 12, 1999, M_w 6.1; August 28, 2002, M_w 6.2; June 24, 2006, M_w 6.3; March 15, 2015, M_w 6.1; April 12, 2019, M_w 6.9; and July 26, 2021, M_w 6.2, which were also located in the neighborhood of the study area (Table S1). The M_w 6.1 (2015) event ruptured with a normal fault mechanism and may lie on the same or similar fault system to the 2021 events. Figure S1 shows all earthquake focal mechanisms from the GCMT catalog in the time range 1976–2024; in addition to the $M_w \geq 6$ events discussed above, there are numerous events in the range M_w 5–6, which help emphasize the complex tectonic setting of the north arm of Sulawesi. It remains unclear what caused the M_w 5.7 earthquake off the coast of Central Sulawesi due to a lack of data.

Deformation within Sulawesi is controlled by two major tectonic systems: the North Sulawesi subduction zone, which accommodates southerly subduction of the Celebes Sea and has a convergence rate of 42–50 mm/year, and the NW–SE trending Palu-Koro fault with a slip-rate of 42 mm/year ([Socquet et al. 2006](#)). A number of previous studies have been conducted in Sulawesi aimed at probing its recent tectonic evolution and geodynamic setting, including focal mechanism inversion ([Greenfield et al. 2021](#)), seismic tomography ([Wehner et al. 2022](#)), dynamic rupture analysis ([Ulrich et al. 2019](#)), seismic hazard analysis ([Cipta et al. 2017](#)), nowcasting analysis ([Pasari et al. 2021](#)), and paleo-seismic investigations ([Natawidjaja and Daryono 2015](#)).

In this study, we propose the existence of a new and previously unidentified fault system in Central Sulawesi through hypocenter relocation of recent earthquakes using an updated 1-D velocity model. We also determine source mechanisms for the M_w 5.7 foreshock, M_w 6.2 mainshock, and subsequent M_w 5.8 event using kinematic inversion. We then calculate the static stress change caused by the M_w 6.2 earthquake in order to investigate the role of stress transfer in the rupture of the M_w 5.8 earthquake.

Data and methods

Data

We use seismic body wave arrival times (direct P- and S-phases) from the BMKG earthquake catalog for earthquake relocation. The initial hypocenters were determined by using the linearized inversion scheme LocSAT ([Bratt and Nagy 1991](#)) with IASP91 as the velocity model ([Kennett and Engdahl 1991](#)). We first select the hypocenter criteria, which include (1) the number of phases must be at least 7 with a minimum of 3 S-phases; (2) hypocenter depth must lie in the range 0–100 km; (3)

azimuthal gap must be $< 180^\circ$; and (4) the epicentral distance to the recording station is $< 5^\circ$. From these criteria, we identified a total of 493 events associated with 7934 P-phases and 2165 S-phases detected by 41 stations of the Indonesian seismic network. The total number of picks for each station is shown in Fig. 2a. For focal mechanism inversion, 3-component waveforms from nearby BMKG stations are exploited. We compiled the seismic waveform data from the stations that are located in the 0–1000 km distance range from the epicenter. We carefully checked the waveform quality and discarded data that have time gaps, off-scale amplitudes, low signal-to-noise ratio, and did not show clear body-wave phases. Furthermore, the inversion was applied to entire waveforms that span 100 s before to 300 s after the P-wave arrival time.

Velocity model

We generated random initial models for use as starting models in the inversion of P- and S-wave arrival times for hypocenter location and 1-D velocity by applying the *Velost* program ([Kissling et al. 1994](#)). By using multiple initial models, a total of 100 initial models with good fit to the data were produced during the inversion process, but ultimately, we chose a small ensemble of the best fitting models to produce an average model (red lines in Fig. 3a) for input into the hypocenter relocation procedure.

Hypocenter relocation

Hypocenters were relocated by employing the double difference method ([Waldhauser and Ellsworth 2000](#)) to obtain more precise locations compared to the BMKG catalog, which were determined using the LocSAT linearized inversion algorithm ([Bratt and Nagy 1991](#)) contained in the *SeisComP3* package ([Hanka et al. 2010](#)). The double difference parameters used in this study consist of a maximum hypocentral separation of 30 km, maximum number of neighbors per event of 50, and minimum number of neighboring phases equal to 8. These values were determined via trial and error, and overall, we found that they delivered good event clustering and data fits. The damping parameter was set at a value of 20 to give a condition number between 40 and 80 for most of the hypocenters obtained, as suggested by [Waldhauser \(2001\)](#). We applied a statistical resampling scheme based on the bootstrap method ([Efron 1982](#)) to assess the uncertainty of the relocated hypocenters. Gaussian noise with a standard deviation of 0.1 s was added to all initial residuals to produce the synthetic data, which were then used to relocate all events, before computing perturbations in the relative mislocations from the reference double-difference locations. The process was repeated 200 times, allowing for the estimation of error ellipsoids

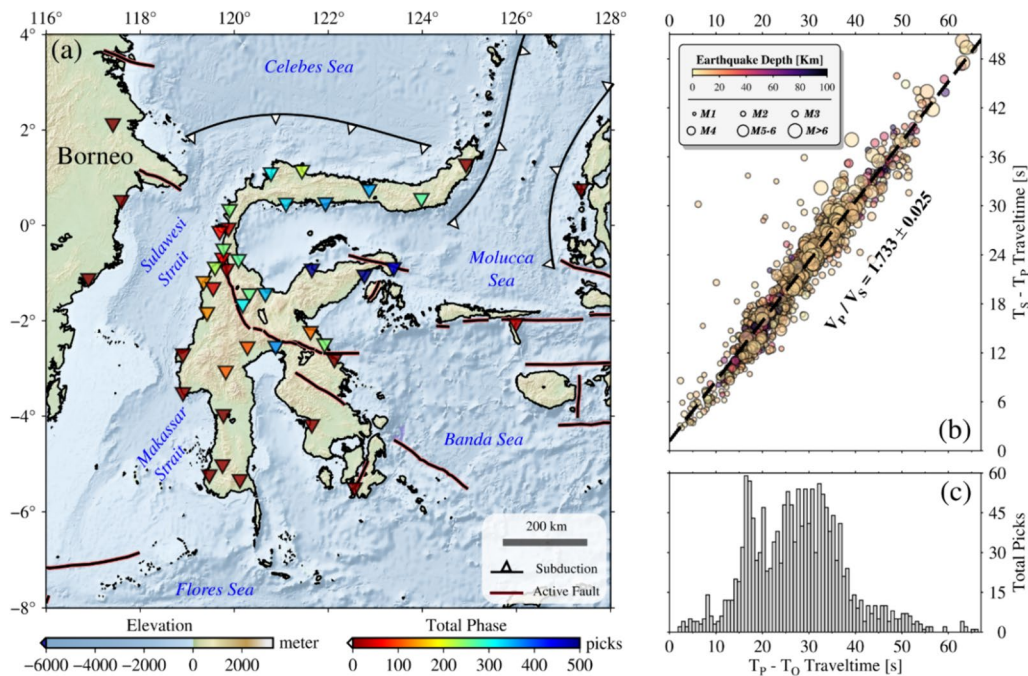


Fig. 2 **a** The BMKG station distribution in Sulawesi within the range of 0–5° (~ 500 km) from the center of the study region, and color-coded to show the number of phases recorded by each station. **b** The Wadati diagram for all earthquakes, which suggests a V_p/V_s ratio of 1.733 ± 0.025 . **c** The histogram of total picks vs travel-time. Most traveltimes range between 20–40 s due to there being fewer stations near the epicenter

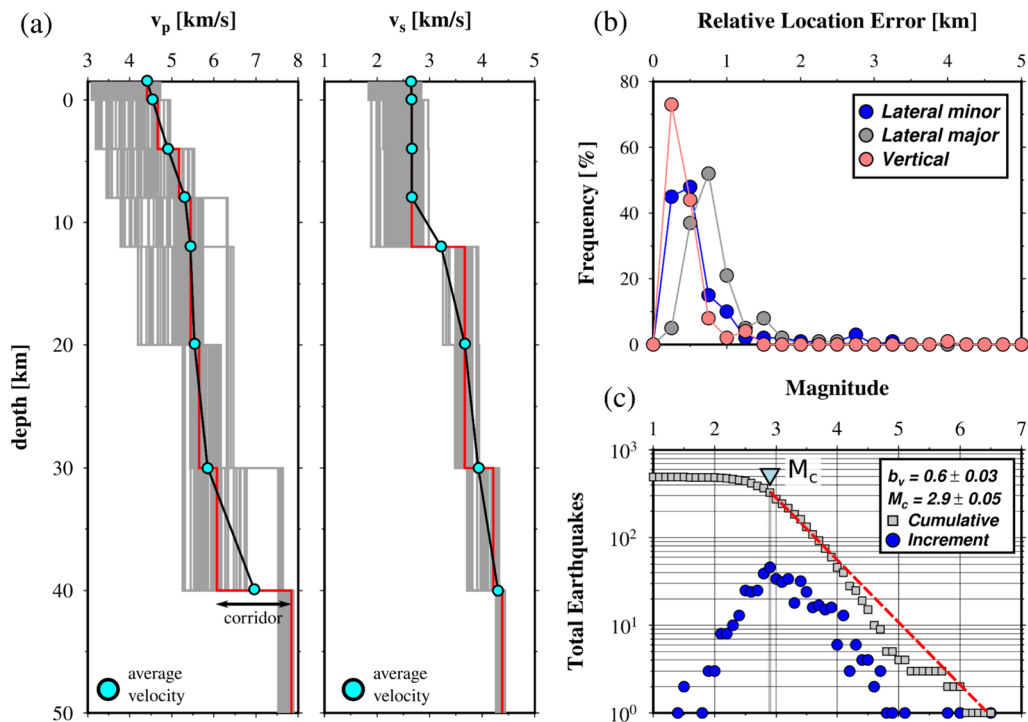


Fig. 3 **a** V_p and V_s as a function of depth for 100 velocity models after coupled hypocenter-velocity inversion using VELEST. The grey lines represent inversion outputs for different initial models. The red lines denote the best fitting V_p and V_s models. The solid line defines the linear interpolation between two values at each depth within the boundaries of the maximum and the minimum velocity range. **b** Relative location error (for an error ellipsoid) is determined using a bootstrap method after hypoDD processing. **c** The frequency–magnitude–relationship reveals a magnitude of completeness (M_c) of 2.90 ± 0.05 and b -value 0.60 ± 0.03

at the 95 percent confidence level for each event. We also used all detected earthquakes from 2021 in Central Sulawesi to determine magnitude of completeness (M_c) and b-value, which are a function of the tectonic stress regime (e.g., Wu et al. 2018) and the capability of the seismic network to detect earthquakes.

Focal mechanisms

We analyzed earthquake source mechanisms using Kiwi Tools (Heimann 2011) and performed a kinematic inversion via the Rapidinv algorithm that is based on a multi-step procedure (Cesca et al. 2010). In our application, we assume a double-couple source mechanism in the inversion and exploit full-waveform recordings from BMKG broadband seismic stations at epicentral distances up to 600 km. The inversion was performed by fitting all three components of the seismogram (vertical, N–S and E–W) in a two-step process using different filters. The first step involves a frequency domain inversion that attempts to fit the amplitude spectra by adjusting fault strike, dip, and rake. The second step involves a time domain inversion of displacement waveforms for centroid coordinates and event onset time. The synthetic seismograms are based on the IASP91 model from the precalculated Kiwi Green's function database (Cesca et al. 2010), and both inversion steps apply a grid search to solve the inverse problem with an L1 misfit function. The Kiwi Tools has been commonly applied in different tectonic system in Indonesia (e.g., Simanjuntak et al. 2023, Muksin et al. 2023, Simanjuntak and Ansari 2024). For all earthquakes we used a frequency range of 0.01–0.05 Hz for the first inversion step and 0.01–0.06 Hz (e.g., Supendi et al. 2022; Adi et al. 2024) for the second inversion step. We used a low frequency range to stabilize the inversion process and minimize the effects of shallow heterogeneity, which are not present in the IASP91 reference model we use.

Static stress change

We used the focal mechanism solution of the Mw 6.2 mainshock to calculate the static Coulomb stress change of the co-seismic slip with Coulomb 3.4. We estimated the stress changes for the optimal normal mechanism at 10.5 km depth by assuming a friction coefficient of 0.4 and a Poisson ratio of 0.25 (Toda et al. 2011) as frequently assumed in static stress change studies (Toda & Stein 2013), especially for previously unidentified faults (Lin & Stein 2004). The proposed fault dimensions and overall fault slip for a normal faulting mechanism were estimated from an empirical scaling relation (Thingbaijam et al. 2017) resulting in a 19 km × 12 km rupture surface for the Mw 6.2 earthquake with an associated 0.4 m average slip. The source dimension of the foreshock is 16 km × 13 km with 0.19 m average slip.

Results

Velocity model

We performed a coupled hypocenter-1-D velocity profile inversion using 100 different starting models obtained by (uniformly) randomly perturbing the reference velocity model (grey lines in Fig. 3a) in the range 5–20%. Based on a simultaneous inversion, we obtain the best-fit velocity model by choosing the solution with the smallest RMS misfit, as shown by the red line in Fig. 3a. The chosen V_p and V_s models exhibit monotonic increases in velocity with depth, and exhibits more detail than the IASP91 model within the same depth range. The final velocity model is represented by an average of the five best fitting models that produce the lowest root-mean-square (RMS) arrival time fit of 0.3 s for P-phase and 0.5 s for S-phase, respectively. Although V_p and V_s increase with depth, the V_p/V_s ratio remains stable with a value of ~ 1.73 .

Magnitude of completeness

Based on our analysis of all events that occurred in 2021, the magnitude of completeness (M_c) is 2.90 ± 0.05 and the corresponding b-value is 0.60 ± 0.03 (Fig. 3b), based on the unrelocated catalog. This result is likely related to the uneven regional station coverage being insufficient to capture lower magnitude events. Note, however, that we only used one year of data from 2021 in the study area and its neighborhood to compute these figures, with all events of $M_w > 1.5$.

Earthquake relocation

During double difference earthquake relocation using HypoDD, as many as 88% of the total number of earthquakes were relocated, with 12% discarded due to their final location being above the surface (a consequence of data noise, data coverage and an imperfect reference model). The relocation results show significant changes in earthquake distribution and exhibit an RMS misfit of 0.0–0.5 s. The events that had previously been held fixed at 10 km depth in the BMKG catalog have now been relocated across a range of depths. The location errors based on the bootstrap analysis method described in the previous section, which are more robust in a relative rather than absolute sense, are shown in Fig. 3b. The average horizontal and vertical mislocations are less than 2 km with a $\sim 90\%$ confidence level (represented by the longest radius of the ellipse), and the corresponding maximum mislocations are less than 5 km (Fig. 3b and S2). However, the relatively poor coverage of stations to the east (see Fig. 2a) appears to produce larger errors—on average—in the E–W direction (4 km) compared to the N–S

direction (3.5 km), although, the uncertainty in the depth direction is greatest overall (5.5 km).

Focal mechanisms

We determined focal mechanism solutions for the three primary earthquakes in the 2021 sequence (Fig. 4). The focal mechanism solutions for the Mw 5.7 foreshock and Mw 6.2 mainshock correspond to normal faults, while

the subsequent Mw 5.8 event occurred on a strike-slip fault. Due to complexity of the updated 1-D seismic velocity model, which was derived from relatively short period arrival times, we used a simplified global model (IASP-91) for the focal mechanism inversion, which used much longer period waveform data (>20 s period). This resulted in a better fit between predicted and observed waveforms (see Fig. S5). The double couple parameters

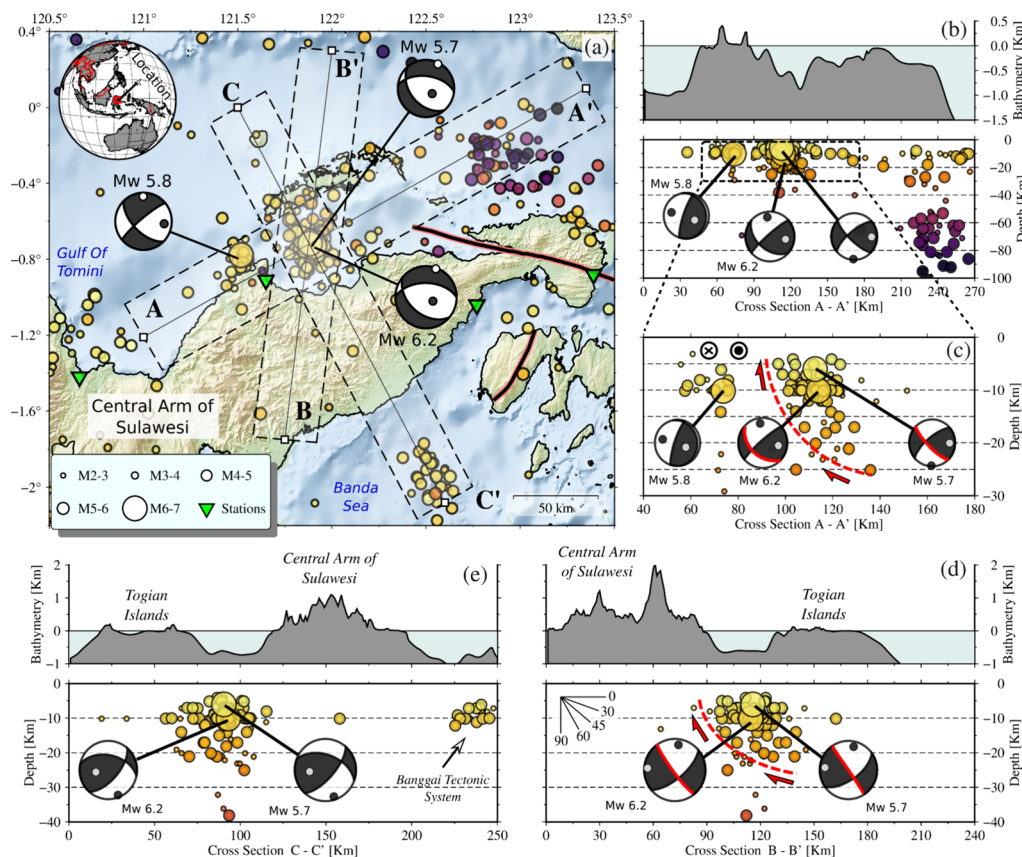


Fig. 4 a Three slices (A–A’, B–B’, and C–C’) depicting the relocated earthquakes and true nodal planes of the Mw 5.7 foreshock, Mw 6.2 mainshock, and Mw 5.8 event in the associated vertical profiles. b The A–A’ cross section shows the earthquakes distributed at shallow depths with normal mechanisms for the Mw 5.7 foreshock and Mw 6.2 mainshock, while the subsequent Mw 5.8 event has a strike-slip mechanism. c The zoom-in of the A–A’ cross section only depicts the two aftershock clusters of the 2021 Tojo Una-Una earthquake in the distance range of 40–140 km (removing non-associative events): (1) cluster arising from the foreshock and mainshock with dip decreasing with depth; (2) cluster arising from the aftershock characterized by vertical dipping. d The B–B’ slice shows a possible ~45° dip of the extension of the Central Balantak fault to the northeast beneath Togian Islands. e The C–C’ cross section shows associated events with the Balantak Fault as well as the Banggai tectonic system that is separated by the Central Arm of Sulawesi

Table 1 Focal mechanism solution data for the three earthquakes examined in this study

Date	Time (UTC)	Mw	Strike1 (deg)	Dip1 (deg)	Rake1 (deg)	Strike2 (deg)	Dip2 (deg)	Rake2 (deg)	DC (%)	CLVD (%)
26/07/2021	03:52:03	5.7	139	44	−57	277	54	−117	93	7
26/07/2021	12:09:07	6.2	130	45	−60	270	52	−116	91	9
26/08/2021	02:14:21	5.8	135	60	−10	230	81	−150	95	5

for these events are shown in Table 1. The observed versus synthetic waveforms for the Mw 5.7 foreshock, Mw 6.2 mainshock, and Mw 5.8 earthquake are shown in Figs. S4–S6. The grid search for focal parameters and comparison results using higher frequency range are shown in Figs. S7–S9. The mainshock focal mechanism solution is in general agreement with the other focal mechanism solutions provided by the USGS, GFZ, GCMT, and IGP as shown in Tables S2, S3 and S4. The difference in centroid depth and horizontal location are 2–3 km and ~0.1°, respectively. However, our event location benefitted from the use of local and regional stations and appears more closely aligned with the fault system responsible for their generation.

Based on the distribution of the relocated hypocenters, two separate clusters are clearly revealed that include the Mw 5.7 foreshock and Mw 6.2 mainshock in the first cluster and the Mw 5.8 event in the second cluster, as shown in Fig. 4a. Cross sections B–B' and C–C' illustrate the first cluster and cross section A–A' reveals the second cluster. The first cluster consists of two normal faulting mechanisms that dip to the northeast (at 40°–50°)

beneath Togian Islands along a WNW–ESE trending fault, as seen in slice B–B' (Fig. 4d). The C–C' slice cross-cuts the earthquakes associated with the Banggai Thrust in the southern part of the study region (Fig. 4e). The Mw 5.7 foreshock and Mw 6.2 mainshock have a similar faulting mechanism and likely occur on the previously unidentified normal fault system that we have called the Central Balantak Fault. Our proposed fault is also supported by the slice A–A' that shows fewer hypocenters beyond ~20 km east of the Mw 6.2 cluster (Fig. 4e). The Mw 5.8 event reflects the presence of a sinistral strike-slip fault that we call the West Balantak Fault.

Static stress change

The static stress changes, using a strike-slip fault as the receiver fault, caused by the Mw 6.2 mainshock depicts areas with increased stress (red color in Fig. 5a) to the NE and SW of the mainshock, while the areas that have decreased Coulomb stress (blue color in Fig. 5a) are to the north and south of the mainshock. The distribution of the mainshock energy release immediately reduced the stress at the hypocenter location; this stress then

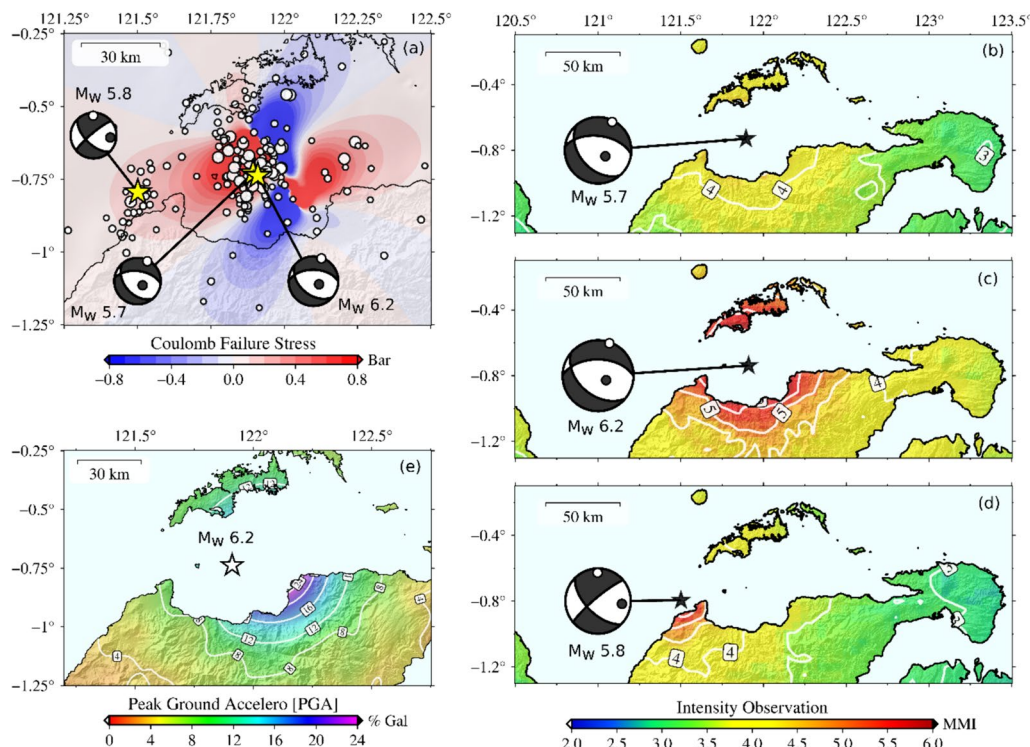


Fig. 5 a Modeled Coulomb stress change caused by the Mw 6.2 mainshock for an optimal normal fault at ~10.5 km depth, with the receiver fault corresponding to the subsequent Mw 5.8 strike-slip fault. The yellow stars and white circles denote the foreshock, mainshock, and associated aftershocks, respectively. The white dots indicate relocated earthquakes and are not color-coded by depth. The earthquakes are mostly distributed in the region of positive stress change (red colors). **b** MMI III–IV caused by Mw 5.7 foreshock. **c** MMI IV–VI caused by Mw 6.2 mainshock. **d** MMI IV–V caused by Mw 5.8 event. **e** An elevation map with peak ground acceleration superimposed, which shows the % PGA in the range of 0–24% gal as a result of the Mw 6.2 mainshock. The intensity and Peak Ground Acceleration (PGA) of the three earthquakes were taken from the BMKG database (www.shakemap.bmkg.go.id)

transferred to the west and initiated the aftershock sequence featuring strike-slip rupture, since these areas experienced a high static Coulomb stress change (up to 1 Bar). In addition, the high static Coulomb stress also transferred to the center and northwest region close to the Balantak Fault that was associated with a significant number of aftershocks.

Ground shaking

To understand the effects of ground shaking, we map the intensity and Peak Ground Acceleration (PGA) of the three earthquakes that were taken from the BMKG database (www.shakemap.bmkg.go.id) (see Fig. 5b–d). The intensity of the three earthquakes is different due to the typical magnitude and distance to the epicenter. The Mw 5.7 foreshock generated MMI III–IV (Fig. 5b), the Mw 6.2 mainshock generated MMI IV–VI (Fig. 5c), and the Mw 5.8 event generated III–V MMI (Fig. 5d). The Mw 6.2 mainshock caused many buildings to collapse on victims because of the poor building construction in the area.

Discussion

We propose a schematic of the responsible fault system in the study area (Fig. 6) based on the Mw 6.2 and Mw 5.8 earthquakes. The fault geometry interpretation is derived from the distribution of seismic activity, the moment tensor solution of the mainshock and major aftershocks, and limited seismic reflection lines (Pholbud et al. 2012). Information on the fault is limited and there is poor bathymetric resolution in the area. We used a maximum stress orientation (S_{Hmax}) based on the world stress map (Heidbach et al. 2016) in the region that exhibits an azimuth of N105°E (Fig. 6a) with a normal stress regime (maximum principal stress is vertical, see Figs. S11–S12). Based on Andersonian stress, the faults lines deviate by approximately 20°–30° to the maximum stress horizontal direction. Watkinson (2011) has identified a number of fault systems in Sulawesi using geological mapping. Furthermore, the National Center for Earthquake Studies of Indonesia (Pusat Studi Gempa Nasional/PuSGeN), as the official group for seismic hazard analysis in Indonesia, has provided limited mapping of the Balantak Fault system onshore. However, the seismic activity along this fault is not well understood from previous studies with less seismicity along 20 km length in the western part (Fig. S16).

Central Sulawesi is divided by the northwest–southeast trending Palu–Koro Fault and its central-western section appears to act as a rigid block system with low seismic activity (Stevens et al. 1999). Recently, there were two interesting events in the western central section, consisting of the Mamasa swarm in 2018 (Supendi et al. 2019) and the Mw 6.2 Mamuju earthquake in 2021 (Supendi

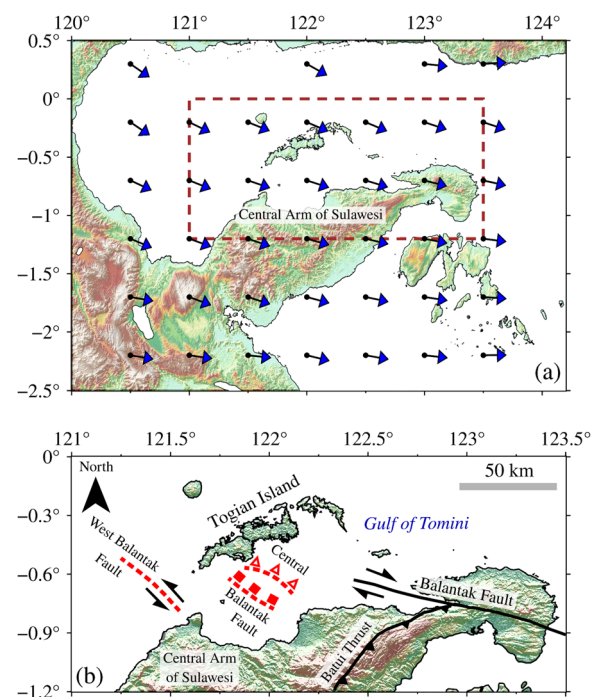


Fig. 6 **a** Maximum horizontal stress orientation derived from the interpolated world stress map (Heidbach et al. 2016) in the central part of Sulawesi. **b** Proposed faults (dashed red lines) for Central and West Balantak fault that ruptured to produce the Mw 6.2 and Mw 5.8 events, as determined by this study. The other fault system defined with black lines was taken from Irsyam et al. (2017)

et al. 2021). The eastern central sector accommodates northeast–southwest-oriented extension according to GPS results (Socquet et al. 2006); this is consistent with major normal-faulting earthquakes that strike in the northwest–southeast direction (Wang et al. 2019). Moreover, Wang et al. (2019) studied the 2017 Mw 6.6 Poso earthquake and found that the extension system in central Sulawesi may be the result of gravitational collapse in two phases, i.e., mass accumulation in the late Miocene–early Pliocene and mass divergence during the Quaternary. However, close proximity (~150 km) between Poso and Tojo Una-una earthquake (Fig. S9) does not provide any link to gravitational collapse caused by a complex tectonic system. Therefore, further studies must be conducted, which are beyond the scope of this study.

The Mw 5.8 event also occurred on a previously unidentified fault that we call the West Balantak Fault (see Fig. 6b). We propose that this fault has a left-lateral mechanism and a NW–SE strike. A fault striking NE–SW is also possible but is very unlikely based on the regional stress. The orientation of the regional stress field tends to clamp the fault and the seismicity around the Mw 5.8 event could be caused by off-fault fracture activation that has an orientation of $\pm 30^\circ$ from the main

fault (Palgunadi et al. 2024). The evidence from high-resolution bathymetry derived from an active seismic reflection survey (Pholbud et al. 2012) also shows lineation of high topography striking NW–SE. The static stress transfer from the Mw 6.2 mainshock may have triggered this event as shown by the Coulomb stress change with the Mw 5.8 rupture acting as the receiver fault. The static stress increase is approximately 0.3 bar. Considering that the azimuth of the maximum horizontal stress is N105° E, the proposed West Balantak Fault is optimally oriented (~20°) (Toda et al. 2011). The shear stress on the West Balantak Fault increases (0.3 bar, Fig. S11d) in accordance with unclamping stress (–0.2 bar, Fig. S11e) which decreases the fault strength and may nucleate the rupture. However, further source studies using results from geodetic, geological, and marine geophysical imaging must be undertaken in future to more comprehensively understand the extension system in central Sulawesi and its consequences for earthquake hazard.

Conclusion

We studied the 2021 eastern central Sulawesi earthquake sequence to locate the previously undetected faults that ruptured. We found two clusters that show a different mechanism in the Central Arm of Sulawesi and determine the presence of what we call the Central Balantak Fault, which has a WNW–ESE strike and a NE dip of ~40–50°. Another fault further to the west is associated with fewer earthquakes and has left-lateral movement; we call this the West Balantak Fault and it also strikes NW–SE. Static stress transfer caused by the Mw 6.2 mainshock along the Central Balantak Fault may have triggered the Mw 5.8 earthquake on the West Balantak Fault. Both faults appear to be part of a complex fault system in Central Sulawesi that ultimately accommodates extension. We acknowledge that the interpretation in this study has some limitations, partly due to a lack of high-resolution bathymetric and geological data, which could help corroborate the existence of the faults we identify from the seismicity.

Supplementary Information

The online version contains supplementary material available at <https://doi.org/10.1186/s40562-024-00353-7>.

Supplementary Material 1.

Acknowledgements

We thank the Agency for Meteorology, Climatology, and Geophysics (BMKG) of Indonesia for granting access to the earthquake data used in this research. The fault data are taken from Irsyam et al. (2017). All figures were made using The Generic Mapping Tools version 6 (Wessel et al. 2019).

Author contributions

A.V.H.S, K.H.P, P.S., U.M., E.G., S.W., N.R., conceived the study; A.V.H.S, K.H.P, P.S., S.W., N.R. contributed to the writing of the manuscript. All authors contributed to the preparation of the manuscript.

Funding

This research is funded by the 2022 Indonesian Collaborative Research of Bandung Institute of Technology awarded to S.W. and was supported by the University of Cambridge through a Herchel Smith Research Fellowship awarded to P.S. This research is also supported by British Council (Newton Fund) Grant G107511 awarded to N.R. Konsorsium Gempabumi dan Tsunami BMKG 2024 is also acknowledged for their support.

Availability of data and materials

Earthquake data are available from the authors upon request.

Declarations

Competing interests

We declare that we have no competing financial, professional or personal interests that might have influenced the performance or presentation of the work described in this manuscript.

Received: 3 July 2023 Accepted: 31 July 2024

Published online: 14 August 2024

References

- Adi SP, Simanjuntak AVH, Supendi P et al (2024) Different faulting of the 2023 (Mw 5.7 and 5.9) South-Central Java earthquakes in the Backthrust fault system. *Geotech Geol Eng.* <https://doi.org/10.1007/s10706-023-02720-1>
- Bao H, Ampuero J-P, Meng L, Fielding EJ, Liang C, Milliner CWD, Feng T, Huang H (2019) Early and persistent supershear rupture of the 2018 magnitude 7.5 Palu earthquake. *Nat Geosci* 12:200–205. <https://doi.org/10.1038/s41561-018-0297-z>
- Bratt SR, Nagy W. (1991) The LocSAT program. Science Applications International Corporation (SAIC)
- Cesca S, Heimann S, Stammler K, Dahm T (2010) Automated procedure for point and kinematic source inversion at regional distances. *J Geophys Res* 115:B06304. <https://doi.org/10.1029/2009JB006450>
- Cipta A, Robiana R, Griffin JD, Horspool N, Hidayati S, Cummins PR (2017) A probabilistic seismic hazard assessment for Sulawesi, Indonesia. *SP* 441:133–152. <https://doi.org/10.1144/SP441.6>
- Daniarsyad G, Sianipar D, Heryandoko N, Priyobudi P (2021) Source mechanism of the 29 May 2017 Mw 6.6 Poso (Sulawesi, Indonesia) earthquake and its seismotectonic implication. *Pure Appl Geophys* 178:2807–2819. <https://doi.org/10.1007/s00024-021-02779-y>
- Efron B (1982) The Jackknife, the bootstrap and other resampling plans, Society for Industrial and Applied Mathematics. <https://doi.org/10.1137/1.9781611970319>
- Greenfield T, Copley AC, Caplan C, Supendi P, Widiyantoro S, Rawlinson N (2021) Crustal deformation and fault strength of the Sulawesi subduction zone. *Tectonics.* <https://doi.org/10.1029/2020TC006573>
- Hanka W, Saul J, Weber B, Becker J, Harjadi P, GITEWS Seismology Group (2010) Real-time earthquake monitoring for tsunami warning in the Indian Ocean and beyond. *Nat Hazards Earth Syst Sci* 10:2611–2622. <https://doi.org/10.5194/nhess-10-2611-2010>
- Heidbach O, Rajabi M, Reiter K, Ziegler M, WSM Team (2016) World Stress Map Database Release 2016, GFZ Data Services. <https://doi.org/10.5880/WSM.2016.001>
- Heimann S (2011) A robust method to estimate kinematic earthquake source parameters, PhD Thesis, University of Hamburg. <http://ediss.sub.uni-hamburg.de/volltexte/2011/5357/>
- Irsyam M, Widiyantoro S, Natawidjaya DH, Meilano I, Rudyanto A, Hidayati S, Triyoso W (2017) *Peta sumber dan bahaya gempa Indonesia tahun 2017.*, Pusat Penelitian dan Pengembangan Perumahan dan Permukiman, Kementerian Pekerjaan Umum dan Perumahan Rakyat (in Indonesian)

- Kennett BLN, Engdahl ER (1991) Traveltimes for global earthquake location and phase identification. *Geophys J Int* 105:429–465. <https://doi.org/10.1111/j.1365-246X.1991.tb06724.x>
- Kissling E, Ellsworth WL, Eberhart-Phillips D, Kradolfer U (1994) Initial reference models in local earthquake tomography. *J Geophys Res* 99:19635–19646. <https://doi.org/10.1029/93JB03138>
- Lin J, Stein RS (2004) Stress triggering in thrust and subduction earthquakes and stress interaction between the southern San Andreas and nearby thrust and strike-slip faults: stress triggering and fault interaction. *J Geophys Res*. <https://doi.org/10.1029/2003JB002607>
- Muksin U, Arifullah A, Simanjuntak AV, Asra N, Muzli M, Wei S, Gunawan E, Okubo M (2023) Secondary fault system in Northern Sumatra, evidenced by recent seismicity and geomorphic structure. *J Asian Earth Sci* 245:105557. <https://doi.org/10.1016/j.jseas.2023.105557>
- Natawidjaja DH, Daryono MR, PrasetyaUdrek G, Liu PL-F, Hananto ND, Kongko W, Triyoso W, Puji AR, Meilano I, Gunawan E, Supendi P, Pamumpuni A, Irsyam M, Faizal L, Hidayati S, Sapiie B, Kusuma MA, Tawil S (2020) The 2018 Mw7.5 Palu ‘supershear’ earthquake ruptures geological fault’s multi-segment separated by large bends: results from integrating field measurements, LiDAR, swath bathymetry, and seismic-reflection data. *Geophys J Int*. <https://doi.org/10.1093/gji/ggaa498>
- Natawidjaja DH, Daryono MR (2015) The Lawanopo Fault, central Sulawesi, East Indonesia, p. 030001, Presented at the national physics conference 2014 (PERFIK 2014). <https://doi.org/10.1063/1.4915009>
- Palgunadi KH, Gabriel AA, Garaqash DI, Ulrich T, Mai PM (2024) Rupture dynamics of cascading earthquakes in a multiscale fracture network. *J Geophys Res Solid Earth* 129(3):e2023JB027578. <https://doi.org/10.1029/2023JB027578>
- Pasari S, SimanjuntakNeha AVH, Sharma Y (2021) Nowcasting earthquakes in Sulawesi Island, Indonesia. *Geosci Lett*. 8:27. <https://doi.org/10.1186/s40562-021-00197-5>
- Pholbud P, Hall R, Advokaat E, Burgess P, Rudyawan A (2012) A new interpretation of Gorontalo Bay, Sulawesi. Proceedings Indonesian Petroleum Association, 36th Annual Convention, IPA12-G-039 1–23
- Simanjuntak VH, Ansari K (2024) Multivariate hypocenter clustering and source mechanism of 2017 Mw 6.2 and 2019 Mw 6.5 in the South Seram subduction system. *Geotech Geol Eng*. <https://doi.org/10.1007/s10706-024-02780-x>
- Simanjuntak AVH, Palgunadi KH, Supendi P, Daryono D, Prakoso TA, Muksin U (2023) New insight on the active fault system in the halmahera volcanic arc, Indonesia, derived from the 2022 Tobelo Earthquakes. *Seismol Res Lett* 94(6):2586–2594. <https://doi.org/10.1785/0220230006>
- Socquet A, Simons W, Vigny C, McCaffrey R, Subarya C, Sarsito D, Ambrosius B, Spakman W (2006) Microblock rotations and fault coupling in SE Asia triple junction (Sulawesi, Indonesia) from GPS and earthquake slip vector data. *J Geophys Res*. <https://doi.org/10.1029/2005JB003963>
- Stevens C, McCaffrey R, Bock Y, Genrich J, Endang, Subarya C, Puntodewo SSO, Fauzi, Vigny C (1999) Rapid rotations about a vertical axis in a collisional setting revealed by the Palu Fault, Sulawesi, Indonesia. *Geophys Res Lett* 26:2677–2680. <https://doi.org/10.1029/1999GL008344>
- Supendi P, Nugraha AD, Widiyantoro S, Abdullah CI, Puspito NT, Palgunadi KH, Daryono D, Wiyono SH (2019) Hypocenter relocation of the aftershocks of the Mw 7.5 Palu earthquake (September 28, 2018) and swarm earthquakes of Mamasa, Sulawesi, Indonesia, using the BMKG network data. *Geosci Lett*. 6:18. <https://doi.org/10.1186/s40562-019-0148-9>
- Supendi P, Nugraha AD, Widiyantoro S, Pesicek JD, Thurber CH, Abdullah CI, Daryono D, Wiyono SH, Shiddiqi HA, Rosalia S (2020) Relocated aftershocks and background seismicity in eastern Indonesia shed light on the 2018 Lombok and Palu earthquake sequences. *Geophys J Int* 221:1845–1855. <https://doi.org/10.1093/gji/ggaa118>
- Supendi P, Ramdhan M, Priyobudi, Sianipar D, Wibowo A, Gunawan MT, Rohadi S, Riama NF, Daryono D, Prayitno BS, Murjaya M, Karnawati D, Meilano I, Rawlinson N, Widiyantoro S, Nugraha AD, Marliyani GI, Palgunadi KH, Elsera EM (2021) Foreshock–mainshock–aftershock sequence analysis of the 14 January 2021 (Mw 6.2) Mamuju–Majene (West Sulawesi, Indonesia) earthquake. *Earth Planets Space* 73:106. <https://doi.org/10.1186/s40623-021-01436-x>
- Supendi P, Rawlinson N, Prayitno BS, Sianipar D, Simanjuntak A, Widiyantoro S, Palgunadi KH, Kurniawan A, Shiddiqi HA, Nugraha AD, Sahara DP, Daryono D, Triyono R, Adi SP, Karnawati D, Daniarsyad G, Ahadi S, Fatchurochman I, Anugrah SD, Heryandoko N, Sudrajat A (2022) A previously unidentified fault revealed by the February 25 2022 (Mw 6.1) Pasaman Earthquake, West Sumatra, Indonesia. *Phys Earth Planet Inter*. <https://doi.org/10.1016/j.pepi.2022.106973>
- Thingbajam KKS, Martin Mai P, Goda K (2017) New empirical earthquake source-scaling laws. *Bull Seismol Soc Am* 107:2225–2246. <https://doi.org/10.1785/0120170017>
- Toda S, Stein RS (2013) The 2011 $M = 9.0$ Tohoku oki earthquake more than doubled the probability of large shocks beneath Tokyo. *Geophys Res Lett* 40:2562–2566. <https://doi.org/10.1002/grl.50524>
- Toda S, Stein RS, Sevilgen V, Lin J (2011) Coulomb 3.3 Graphic-rich deformation and stress-change software for earthquake, tectonic, and volcano research and teaching-user guide (Report No. 2011–1060). Open-File Report, Reston, VA. <https://doi.org/10.3133/ofr20111060>
- Ulrich T, Vater S, Madden EH, Behrens J, van Dinther Y, van Zerst I, Fielding EJ et al (2019) Coupled, physics-based modeling reveals earthquake displacements are critical to the 2018 Palu, Sulawesi Tsunami. *Pure Appl Geophys* 176:4069–4109. <https://doi.org/10.1007/s00024-019-02290-5>
- Waldhauser F (2001) hypoDD-A program to compute double-difference hypocenter locations (Report No. 2001–113). <https://doi.org/10.3133/ofr01113>
- Waldhauser F, Ellsworth WL (2000) A double-difference earthquake location algorithm: method and application to the Northern Hayward Fault, California. *Bull Seismol Soc Am* 90:1353–1368. <https://doi.org/10.1785/0120000006>
- Wang S, Xu C, Xu W, Yin Z, Wen Y, Jiang G (2019) The 2017 Mw 6.6 Poso earthquake: implications for extrusion tectonics in Central Sulawesi. *Seismol Res Lett* 90:649–658. <https://doi.org/10.1785/0220180211>
- Watkinson IM (2011) Ductile flow in the metamorphic rocks of central Sulawesi. *Geol Soc Spec Publ* 355:157–176. <https://doi.org/10.1144/SP355.8>
- Wehner D, Rawlinson N, Greenfield T, Daryono, Miller MS, Supendi P, Lü C, Widiyantoro S (2022) SASSIER2: full-waveform tomography of the eastern Indonesian region that includes topography, bathymetry and the fluid ocean. *Geochem Geophys Geosyst*. <https://doi.org/10.1029/2022GC010563>
- Wessel P, Luis JF, Uieda L, Scharroo R, Wobbe F, Smith WHF, Tian D (2019) The generic mapping tools version 6. *Geochem Geophys Geosyst* 20:5556–5564. <https://doi.org/10.1029/2019GC008515>
- Wu Y-M, Chen SK, Huang T-C, Huang H-H, Chao W-A, Koulakov I (2018) Relationship between earthquake b -values and crustal stresses in a young orogenic belt. *Geophys Res Lett* 45:1832–1837. <https://doi.org/10.1002/2017GL076694>

Publisher’s Note

Springer Nature remains neutral with regard to jurisdictional claims in published maps and institutional affiliations.